35th Annual International Conference of the IEEE EMBS
Osaka, Japan, 3 - 7 July, 2013

Tracking instantaneous pressure-to-flow dynamics of cerebral autoregulation induced by CO2 reactivity*

Jia Liu, *Member, IEEE*, Hesam Koochakpour, Ronney B. Panerai, Emmanuel Katsogridakis, Zuoen Wang, and David M. Simpson

***Abstract*—In this work, we proposed a novel method to investigate the underlying rapid pressure-to-flow dynamics induced by changes of arterial CO2. Autoregulation was modeled as a multivariate system. The instantaneous effect of CO2 to cerebral blood flow velocity (CBFV) was removed adaptively by the recursive least square (RLS) method from CBFV. The residue CBFV and arterial blood pressure (ABP) were then filtered by a Gaussian-modulated sinusoidal pulse filter, in order to optimize the time and frequency resolution when estimating the instantaneous phase difference between the signals using Hilbert transform (HT). The results indicate that the effect of CO2 on dynamic autoregulation is slower than on CBFV.**

I. Introduction

Cerebral autoregulation (CA) is defined as a mechanism that maintains relatively constant cerebral blood flow despite dynamic changes of blood pressure [1]. In short, it is a pressure-to-flow mechanism, although changes in cerebral blood flow can also be induced by other parameters, such as CO2, O2, or sympathetic activity. CO2 is known as a vasodilator that can change blood flow greatly in seconds, which means that the variation of CBFV is partially contributed by CO2 and partially by ABP during changes in arterial CO2. Thus, in order to calculate the phase dynamics, one of the main indicators of CA effectiveness, the partial variation of CBFV induced by CO2 needs to be removed. We therefore used a multivariate structure to model autoregulation as a multiple-input and single-output (MISO) system, where ABP and CO2 are the inputs and CBFV is the output [2]. Considering the time-varying properties of the MISO system during the course of vasodilation/constriction, we chose an RLS adaptive method to extract the partial CBFV with respect to time. The residue CBFV (rCBFV) and ABP can then be used to estimate the phase dynamics.

In order to catch rapid phase dynamics of autoregulation, we chose Hilbert transform to calculate the instantaneous phase difference (PD) between the rCBFV and ABP. It is worth noting that the time and frequency resolution is not determined by the sampling rate of the signals, but the band-pass filter applied to the signals prior to HT. In our case, PD at 0.1 Hz is of interest and the phase dynamics of autoregulation may change in a few seconds, which requires a band-pass filter with a good compromise of time and frequency resolution. Therefore, we proposed a Gaussian pulse filter (GF) modulated by a sinusoidal wave at 0.1 Hz, given that the GF is in a Gaussian shape and minimal spread in both time and frequency domain.

After describing the main system identification techniques, a simulation test was performed to test the proposed methods under controlled conditions. Finally, we applied our main method, in comparison with alternatives, to the signals recorded from 27 healthy volunteers and showed the phase dynamics induced by step-wise changes of end-tidal CO2 (ETCO2).

II. Method

A. Multivariate System

Cerebral autoregulation is modeled as an MISO system, where ABP, $p[n]$, and ETCO2, $c[n]$, are the inputs and CBFV, $v[n]$, is the output [2],

$$v[n] = v_p[n] + v_c[n] = \sum_{i=0}^{L_{pv}-1} h_{pv}[i]p[n-i] + \sum_{j=0}^{L_{cv}-1} h_{cv}[i]c[n-j], \quad (1)$$

where n denotes samples at 1 Hz sampling rate, and $v_p[n]$ and $v_c[n]$ are the partial CBFV correlated with ABP and ETCO2, respectively. $h_{pv}[i]$ and $h_{cv}[i]$ are the causal FIR filter impulse responses, and L_{pv} and L_{cv} denote the orders of the filters, which are 6th and 20th, respectively [2][3].

B. RLS Method

Based on (1), we extended our previous univariate RLS adaptive filter (UAF) to a multivariate RLS adaptive filter (MAF) and updated the filter impulse responses from the signals sample by sample. We first estimated the Kalman gain vectors, $k_p[n]$ and $k_c[n]$,

$$k_p[n] = \frac{\lambda^{-1}\boldsymbol{P}_p[n-1]p[n]}{1+\lambda^{-1}\boldsymbol{x}[n]\boldsymbol{P}_p[n-1]\boldsymbol{x}[n]}, (0 \le \lambda \le 1), \quad (2)$$

$$k_c[n] = \frac{\lambda^{-1}\boldsymbol{P}_c[n-1]c[n]}{1+\lambda^{-1}\boldsymbol{x}[n]\boldsymbol{P}_c[n-1]c[n]}, (0 \le \lambda \le 1), \quad (3)$$

where $\boldsymbol{P}[n] = \boldsymbol{R}_n^{-1}$ is the inverse autocorrelation matrix of the input signals. We then estimated the error at the n-th sample by,

$$e_n[n] = v[n] - \boldsymbol{H}[n-1]^t\boldsymbol{x}[n], \quad (4)$$

*This work is supported by National Natural Science Foundation of China (No. 81000644), Shenzhen-Hong Kong Innovation Circle Project and Shenzhen Fundamental Research Program (JC201005270365A).

Jia Liu is with Guangdong Provincial Key Laboratory of Robotics and Intelligent System, Shenzhen Institutes of Advanced Technology, Chinese Academy of Sciences and the Chinese University of Hong Kong, Shatin, Hong Kong, P. R. China (phone:+86-755-86392138, e-mail: jia.liu@siat.ac.cn).

Ronney B. Panerai and Emmanuel Katsogridakis are with Department of Cardiovascular Sciences, University of Leicester, UK.

Hesam Koochakpour and David M. Simpson are with ISVR, University of Southampton, UK.

Zuoen Wang is with Shenzhen Institutes of Advanced Technology, Chinese Academy of Sciences, Shenzhen, P. R. China.

where $\boldsymbol{H}[n-1]^t$ is

$$\boldsymbol{H}[\boldsymbol{n-1}] = \begin{bmatrix} \boldsymbol{H_{pv}}[\boldsymbol{n-1}] \\ \boldsymbol{H_{cv}}[\boldsymbol{n-1}] \end{bmatrix}, \quad (5)$$

$$\boldsymbol{H_{pv}}[\boldsymbol{n-1}] = \left[\boldsymbol{h_{pv}}[\boldsymbol{0}] \ldots \boldsymbol{h_{pv}}[\boldsymbol{L_{pv}-1}]\right], \quad (6)$$

$$\boldsymbol{H_{cv}}[\boldsymbol{n-1}] = \left[\boldsymbol{h_{cv}}[\boldsymbol{0}] \ldots \boldsymbol{h_{cv}}[\boldsymbol{L_{cv}-1}]\right]. \quad (7)$$

And $\boldsymbol{x}[n]$ is

$$\boldsymbol{x}[\boldsymbol{n}] = \begin{bmatrix} \boldsymbol{x_p}[\boldsymbol{n}] \\ \boldsymbol{x_c}[\boldsymbol{n}] \end{bmatrix}, \quad (8)$$

$$\boldsymbol{x_p}[\boldsymbol{n}] = \left[\boldsymbol{p}[\boldsymbol{n-L_{pv}}] \ldots \boldsymbol{p}[\boldsymbol{n}]\right], \quad (9)$$

$$\boldsymbol{x_c}[\boldsymbol{n}] = \left[\boldsymbol{c}[\boldsymbol{n-L_{cv}}] \ldots \ \boldsymbol{c}[\boldsymbol{n}]\right]. \quad (10)$$

The weight vector $\boldsymbol{H}[n]$ is updated by,

$$\boldsymbol{H}[\boldsymbol{n}] = \boldsymbol{H}[\boldsymbol{n-1}] + \ \boldsymbol{e_n}[\boldsymbol{n}]\boldsymbol{k}[\boldsymbol{n}], \quad (11)$$

where

$$\boldsymbol{k}[\boldsymbol{n}] = \begin{bmatrix} \boldsymbol{k_p}[\boldsymbol{n}] \\ \boldsymbol{k_c}[\boldsymbol{n}] \end{bmatrix}. \quad (12)$$

We then updated the $\boldsymbol{P}[n]$ adaptively for each input,

$$\boldsymbol{P}[\boldsymbol{n}] = \boldsymbol{\lambda^{-1}}\boldsymbol{P}[\boldsymbol{n-1}] - \boldsymbol{\lambda^{-1}}\boldsymbol{k}[\boldsymbol{n}]\boldsymbol{x}[\boldsymbol{n}]^{\boldsymbol{T}}\boldsymbol{P}[\boldsymbol{n-1}]. \quad (13)$$

To this end, the rCBFV with the partial CBFV correlated with ETCO2, $v_c[n]$, removed can be estimated sample by sample as,

$$\boldsymbol{v_r}[\boldsymbol{n}] = \ \boldsymbol{v}[\boldsymbol{n}] - \boldsymbol{H_{cv}^T}\boldsymbol{x_c}[\boldsymbol{n}]. \quad (14)$$

D. Instantaneous Phase Difference using Hilbert Transform

The instantaneous phase difference (PD) can then be estimated between the analytic signals of ABP and the residue CBFV, which are defined as:

$$p^a[n] = p[n] + j\tilde{p}[n] = \mathrm{A}_p[n]e^{j\varphi_p[n]}, \quad (15)$$

$$v_r^a[n] = v_r[n] + j\widetilde{v}_r[n] = A_{v_r}[n]e^{j\varphi_{v_r}[n]}, \quad (16)$$

where $p^a[n]$ and $v_r^a[n]$are the analytic signals, respectively. $\tilde{p}[n]$ and $\widetilde{v}_r[n]$ are the Hilbert transform (HT) of the real signals, $p[n]$ and $v_r[n]$.

As shown above, the analytic signals can also be denoted by its instantaneous amplitude $A[n]$ and instantaneous phase $\varphi[n]$. The instantaneous PD can then be calculated as:

$$\varphi_{v_r}[n] - \varphi_p[n] = \arg\left(\frac{p^a[n]v_r^{a*}[n]}{|p^a[n]||v_r^a[n]|}\right). \quad (17)$$

E. Gaussian-modulated Sinusoidal Pulse Filter (GSPF)

Though the calculation of the instantaneous amplitude and phase using HT may apply to an arbitrary broad-band signal, the physical meaning of these instantaneous parameters becomes clear only when the signal is within a narrow band. Therefore, band pass filtering is generally required prior to HT to extract the signal component of interest. The temporal and frequency resolution of the instantaneous phase is determined by the band-pass filter [4].

Given that Gaussian shape is of minimal spread in both time and frequency domain, we defined a Gaussian-modulated sinusoidal pulse filter, $\mathrm{GF}[n]$, as:

$$\mathrm{GF}[n] = \frac{1}{\sqrt{2\pi\sigma_{gf}}}\sin(2\pi f_c n)\, e^{(-n^2/\sigma_{gf})}, \quad (18)$$

where f_c is the centre frequency and σ_{gf} is the bandwidth parameter, respectively. We set the centre frequency, f_c, at 0.1 Hz, as this is the most relevant frequency to show the phase dynamics of cerebral autoregulation [3]. The bandwidth parameter was chosen to be $\sigma_{gf} = 60$ which was determined by comparing the GSPF with a series of Butterworth band-pass filters at different bandwidths.

F. Simulation Test and Real Data

In order to show the performance of the proposed method in an ideal condition, a simulation test was designed to compare four different methods of estimating time-varying parameters. After the simulation test, the proposed method was then applied to a set of real data.

1) Simulation Test

Step changes of PD were simulated by filtering a sinusoidal wave at 0.1 Hz with Tiecks filters in a sequence of autoregulation index (ARI) at 1, 7, and, 3, where the sinusoidal wave were considered as the simulated ABP, $p^s[n] = \sin(2\pi \cdot 0.1 \cdot n)$, and the filtered signals were the simulated partial CBFV, $v_p^s[n]$, that is correlated to ABP. The simulated ETCO2, $c^s[n] = \sin(2\pi \cdot 0.05 \cdot n)$, was denoted by another sinusoidal wave at 0.05 Hz and a sequence of phase changes (changes at the same time as the ARI) at $\pi/2$, π, and $\pi/2$ used as the simulated, $v_c^s[n] = \sin(2\pi \cdot 0.05 \cdot n + \varphi), \varphi = \frac{\pi}{2}, \pi, \frac{\pi}{2}$. The total simulated CBFV is therefore equal to $v^s[n] = v_p^s[n] + v_c^s[n]$.

We then used the proposed techniques to track the step changes of phase dynamics.

- <u>*GSPF-HT and MAF*</u>: Using MAF, we estimated $v_r^s[n]$ by (14) and then calculated the instantaneous PD between the estimated rCBFV and the simulated $p^s[n]$ using GSPF and HT (GSPF-HT).
- <u>*GSPF-HT and UAF*</u>: Instead of using MAF, we applied only an univariate adaptive filter to estimate $v_r^s[n]$. In this case, there is only one input, $c^s[n]$, and one output, $v^s[n]$, of the system, which means $x_p[n] = 0$ in Equation (2)-(14). We then estimated instantaneous phase using GSPF-HT from this pair of estimated $v_r^s[n]$ and simulated $p^s[n]$.
- <u>*GSPF-HT*</u>: For a comparison, we applied the GSPF-HT techniques directly to $v^s[n]$and $p^s[n]$ to show how the CBFV component from estimated ETCO2 affects the estimated PD.

2) Real Data

Twenty-seven subjects (25-55 years old) were enrolled for continuous recording of ABP, CBFV and ETCO2 (2 recordings for each, 54 in total) at Leicester Royal Infirmary, UK. The study received local ethical committee approval and all subjects gave written informed consent. They were free from known cerebrovascular or cardiovascular diseases. With

subjects in the supine position, ABP was recorded non-invasively using the arterial unloading techniques (Finometer, Ohmeda). Freehand transcranial Doppler (Companion III, Viasys Healthcare) identification of the both middle cerebral arteries (MCA) was performed using 2MHz probe, which was then held in place by a custom built head frame. A face mask was connected to a CO2 delivery system, and by a line to a capnograph (Datex, Normocap 200) to measure end-tidal CO2 (ETCO2) levels.

Step changes of ETCO2 were induced by inhaling a 5% CO2/air mixture from the face mask, resulting in normocapnia (NC), hypercapnia (HC) and then back to normocapnia (NC) (5 minutes for each session). A low-pass filter with cutoff frequency at 0.5 Hz was applied to obtain beat-to-beat changes of ABP and CBFV, which were then down-sampled to 1 Hz. All signals were then filtered by a high-pass filter at 0.01 Hz cutoff frequency to remove the low frequency trends caused by CO2 step changes.

The same methods described in the simulation test were applied to the data for tracking the phase dynamics. In order to compare with the method that we previous proposed for estimating time-varying phase dynamics, we also used an adaptive filter to calculate the phase difference to compare the tracking speed [3]. As the time of CO2 onset and offset was marked during data recording, the estimated PD from each recording was aligned by the starting points of CO2 changes to show the phase dynamics induced by CO2 reactivity.

III. Result

In Fig. 1, it shows that the proposed method (solid line) can track the simulated phase dynamics more closely to the ground truth (dashed line) than the other methods (dashdot and dotted lines). Although we simulated ETCO2 at a different frequency (0.05 Hz) from the ABP (0.1 Hz), without removing the effect of ETCO2 by the adaptive filter, evident ripples can be observed in the estimated instantaneous PD using GSPF-HT alone. However, though effect of ETCO2 is suppressed when we used UAF and GSPF-HT, we found the result is biased from the ground truth. The root-square-error (RSE) between the simulated $v_p^s[n]$and estimated $v_r^s[n]$ by MAF and UAF is shown in Fig. 2.

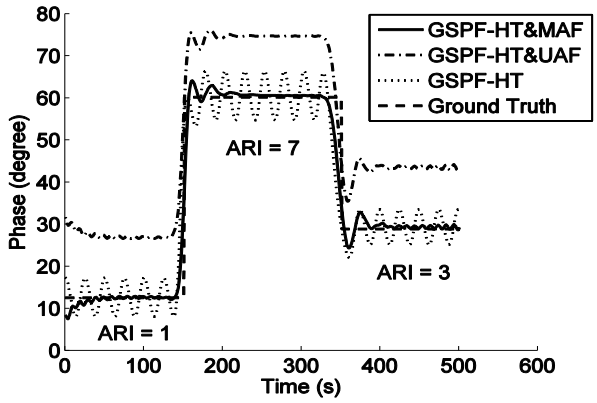

Figure 1. Results of tracking step changes of phase dynamics. 1) Solid line is thePD estimated by GSPF-HT and MAF; 2) Dashdot line is estimated by GSPF-HT and UAF; 3) Dotted line is esitmated by GSPF-HT; 4)Dashed line is the ground truth calculated from Tiecks' model (ARI = 1, 7 , and 3)

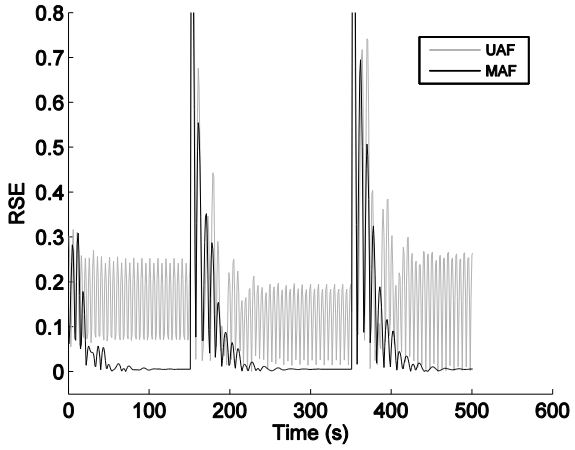

Figure 2. Error analysis of the simulation. The RSE between the simulated $v_p^s[n]$and estimated $v_r^s[n]$by MAF (dark line) and UAF (gray line).

It shows that using MAF the error increases and then drops back to zero when sudden phase change was simulated. However, in the case of UAF, the error does not converge to zero (see explanation in the Discussion), resulting in biased estimate (gray line) of the phase difference in Fig. 1.

Fig. 3-4 show the phase dynamics estimated from the recorded signals. Fifty-four estimated continuous phase dynamics were aligned by CO2 onset and offset (shown by the gaps from the 150th second in Fig. 3-4), which separates normocapnia and hypercapnia. In order to rule out the outliers, we plotted out the median values of the PD calculated across the 54 recordings. It is evident that, without removing the effect of ETCO2, the instantaneous PD (dashed lines) changes dramatically when subjects started and stopped to inhale air mixed with 5% CO2.

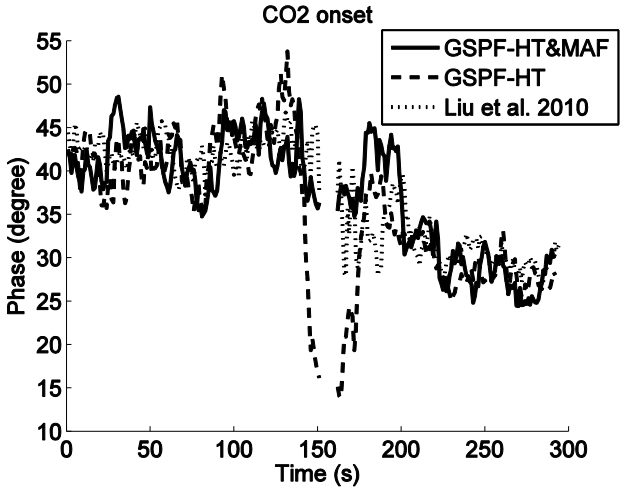

Figure 3. Population median phase dynamics induced by inhaling air mixed with 5% CO2. 1) Solid line is the PD estimated by GSPF-HT and MAF; 2)Dashed line is esitmated by GSPF-HT; 3) Dotted line is estimated by an adaptive filter proposed in [3].The gap denotes the time of CO2 onset.

The sudden changes of phase dynamics during the step-wise CO2 changes can be reduced if we applied MAF (solid lines) (we did not use UAF, as bias was introduced) to remove the partial CBFV introduced by ETCO2 or used an adaptive filter

to estimate the phase dynamics (dotted lines) in a relatively slower tracking speed [3].

Table I-II suggests that all these methods can also be used to grade autoregulation when subjects are in different CO2 levels.

TABLE I. PHASE DIFFERENCE ALIGNED BY CO2 ONSET

	Normocapnia			*Hypercapnia*		
Method	1	2	3	1	2	3
Median±std (degree)	41±18	43±17	43±17	35*±15	30*±12	36*±13

Method 1: GSPF-HT and MAF

Method 2: GSPF-HT

Method 3: Adaptive filter proposed in [3]

*: p<0.01 t-test for comparing PD in normocapnia and hypercapnia

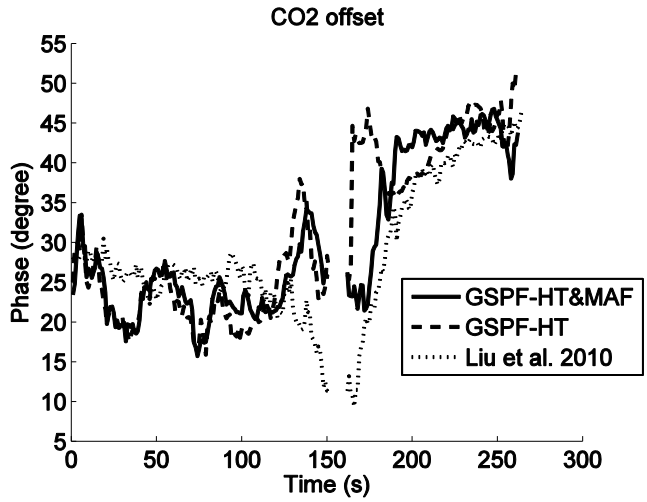

Figure 4. Population medianphase dynamics induced by inhaling ambient air from 5% CO2 mixture. Llines are derived by the same methods in Fig 1. The gap denotes the time of CO2 offset.

TABLE II. PHASE DIFFERENCE ALIGNED BY CO2 OFFSET

	Hypercapnia			*Normocapnia*		
Method	1	2	3	1	2	3
Median±std (degree)	21±12	21±12	26±12	35*±16	33*±14	31*±13

Same footnotes as in TABLE I

IV. DISCUSSION

In this work, we proposed a novel method that can track rapid phase dynamics of cerebral autoregulation. We used MAF to remove the dynamic effect of ETCO2 and then calculated instantaneous phase dynamics of cerebral autoregulation using GSPF-HT from the residue CBFV and ABP.

The simulation results show that this method can track sudden changes of phase difference and suppress the effect from the simulated CO2 in neighbouring frequency bands (0.05 Hz). Although this effect can also be reduced by UAF, biased estimates were observed (Fig. 1). As the simulation is designed specifically for an MISO system, UAF cannot explain all the variation in the simulated CBFV and hence has to compromise in its estimate of the impulse response to minimize the overall error. It is also understandable that we observed ripples (dotted line in Fig. 1) even when a dedicated band-pass filter (GSPF) was applied, as signal components from neighbor frequency bands can leak into the filtered signals if time resolution is demanded.

When the proposed method was applied to the real data, it is evident that the effect of ETCO2 to the phase dynamics is reduced in Fig. 3-4. During CO2 onset and offset, the phase difference drops down (approx. 35 degree) and jumps up (approx. 20 degree), if the partial CBFV induced by ETCO2 is not removed. The results in Fig. 3-4 also indicate that the effect of CO2 on CBFV is relatively fast, whilst the pressure-to-flow dynamics changes gradually afterwards. Before and after the intake of the mixed air, the phase dynamics estimated by different method are similar, implying the partial CBFV from CO2 is weak during these periods and the pressure-to-flow dynamics is dominant.

We also compared the current method with the adaptive method that we previously proposed for assessing time-varying phase dynamics. It shows that the sudden phase is reduced by the adaptive filter. However, the rapid dynamics might have been lost (evident in Fig 4.), as the previous method updates the estimate in a relatively slow speed.

V. CONCLUSION

We provided a novel method to study the underlying rapid pressure-to-flow dynamics induced by multiple cerebral hemodynamic changes (CO2 reactivity, in this case). This method reveals that cerebral autoregulation may not change as quickly as cerebral blood flow when cerebral artery dilated/constricted by increasing/decreasing ETCO2.

REFERENCES

[1] O. Paulson, S. Strandgaard, and L. Edvinsson, "Cerebral autoregulation," *Cerebrovascular and Brain Metabolism Reviews*, vol. 2, p. 161, 1990.

[2] R. Panerai, D. Simpson, S. Deverson, P. Mahony, P. Hayes, and D. Evans, "Multivariate dynamic analysis of cerebral blood flow regulation in humans," *IEEE Transactions on Biomedical Engineering*, vol. 47, pp. 419-423, 2000.

[3] J. Liu, D. M. Simpson, J. Yan, and R. Allen, "Tracking time-varying cerebral autoregulation in response to changes in respiratory PaCO2," *Physiological Measurement,* vol. 31, p. 16, 2010.

[4] A. Bruns, "Fourier-, Hilbert-and wavelet-based signal analysis: are they really different approaches?" *Journal of neuroscience methods,* vol.137(2), p. 321-332 2004.